J Mater Sci: Mater Electron (2023) 34:316

Upcycling of waste printed circuit boards into metallic pyrolytic carbon for supercapacitor electrode

Havva Hande Cebeci[1], İbrahim Yılmaz[2], Önder Yargı[3,6], Korkut Açıkalın[4], Ali Gelir[5], and Aysel Kantürk Figen[1,6,*]

[1] Department of Chemical Engineering, Yildiz Technical University, 34220 Istanbul, Turkey
[2] Department of Metallurgy and Materials Engineering, Yildiz Technical University, Istanbul, Turkey
[3] Department of Physics, Yildiz Technical University, Istanbul, Turkey
[4] Department of Energy Systems Engineering, Yalova University, Yalova, Turkey
[5] Department of Physics, Istanbul Technical University, 34469 Istanbul, Turkey
[6] Clean Energy Technologies Institute, Yıldız Technical University, 34220 Istanbul, Turkey

Received: 3 October 2022
Accepted: 31 December 2022
Published online: 31 January 2023

ABSTRACT

Upcycling of electronic waste is the efficient strategy to minimize the negative effect on environment. In the present study, e-waste (originating from small household appliances) was upcycled into the metal contented pyrolytic carbon (C-WPCB) through a simple pyrolysis without activation or any other additional processes. After crushing and fractionating, pyrolysis was performed at 500 °C under nitrogen atmosphere. The obtained metallic pyrolytic carbon was characterized by well-known techniques such as SEM–EDS, XRF, XRD, ATR/FT-IR, TG/DTG, and BET analyses and utilized for supercapacitor electrode preparation. For this purpose, nickel foam was electrochemically coated by C-WPCB which was previously dispersed in three different solutions: 1.5 M H_2SO_4, 3 M KCl, and 1.5 M KOH, respectively. Electrochemical characterization of the prepared electrodes was performed by cyclic voltammetry (CV) at different scan rates and galvanostatic charge–discharge (GCD) methods at different current densities in 6 M KOH electrolyte in half-cell configuration. The best performance was obtained for the electrode prepared in H_2SO_4 solution where the specific capacitance, specific power, and specific energy were found as 39.5 F/g, 25.0 kW/kg, and 16.5 Wh/kg at 5 A/g, respectively.

1 Introduction

According to the global electronic waste (e-waste) monitor's 2020 data, 53.6 Mt of e-waste was produced in the world in 2019, and an increase of 9.2 Mt has been achieved since 2014 [1]. The rapid expansion of e-waste has affected negatively the environment and human health [2]. Waste printed circuit boards (W-PCB), which constitutes 1.6% of e-waste, provides the connection between software and hardware in

Address correspondence to E-mail: akanturk@yildiz.edu.tr

https://doi.org/10.1007/s10854-023-09817-6

electronic equipment [3]. W-PCB is mainly constituted of Au (0.035%), Cu (22.0%), Pb (1.5%), Sn (2.6%), and non-metals (%45) (such as fiber glass, epoxy resin, and brominated flame retardants) and contains many electronic components in its structure such as resistors, relays, capacitors, transistors, heat sinks, chip lines, and processors [4, 5]. It is classified as single/double-sided and multi-layered. These layers are produced in FR-4 and FR-2 types and exhibit thermoplastic behavior like brominated flame retardants (BFRs). Type FR-4 consists of glass fiber material coated with multilayer epoxy resins and copper layers. It is utilized in small devices such as telecommunication equipment and computers. The FR-2 type consists of a cellulosic paper layer and phenolic-based coated with copper and used especially in television and household goods [6]. W-PCBs, which play an important role in the circular economy, require less energy, and produce less greenhouse gas emissions [7].

Recycling of precious metals in the structure of W-PCB can be done by physical, mechanical, pyrometallurgical, hydrometallurgical, and thermal recycling methods [8]. It is possible to recycle all precious materials (metallic and non-metallic fraction) with pyrolysis, which is one of the thermal recycling methods. Especially, organic compounds (non-metallic fraction) decompose in this process and converted to gaseous, liquid, and solid (char) products in an inert atmosphere through thermal decomposition [7, 9].

Nowadays for a sustainable world, studies on energy storage have accelerated due to the increasing carbon emissions in recent years [10]. Energy storage devices are found in electrical and electronic equipment, renewable energy sources, transportation vehicles, and the medical field [11]. Supercapacitors are a kind of energy storage device that performs between batteries and conventional capacitors. They have high power densities, short charge/discharge times at high speeds, long lifetimes, and minimum rate of extinction compared to batteries, and they can operate at low and high temperatures [12–14].

Electrode materials developed for supercapacitors based on oxide, sulfur, nitride, phosphite, boride, ferrite, and polymers can provide high energy density, but they have poor cycle life and relatively low power density. In contrast, carbon-based electrode materials exhibit excellent life and fast charge/discharge, but their low energy density limits their application [15].

Various carbon-based materials such as activated carbons, mesoporous carbons, carbon nanotubes, and graphene are utilized in the electron material of supercapacitors in recent years. Activated carbon is preferred as an electrode material because it is more environmentally friendly, relatively cost, and more stable than other materials. In addition, it has effective electrical conductivity, high capacitance, high surface area/porosity, and longer cycle life [16–18].

Many researchers have been utilized non-metallic fraction (NMF) separated from waste PCB by pyrolysis char. It investigated activated carbons with high porosity, which were obtained from chars derived from pyrolysis of NMFs in waste paper-based PCBs by using chemical and physical activation methods [19]. Activated carbons have been synthesized by using waste PCBs via physical activation subsequent to pyrolysis processes. The physical and chemical properties of the produced activated carbons were studied using nitrogen adsorption [20]. Highly specific surface area carbon materials derived from the PCB for supercapacitor electrode material are prepared via microwave carbonization and KOH activation process with controlled activation temperature [21].

In recent studies, e-wastes are one of the recommended materials to produce supercapacitor electrodes. Dutta et al. summarized different techniques used to recycling different waste materials in the supercapacitor designs [22]. For example, Nagaraju et al. constructed fiber-type SC by using waste Cu wires [23]. Some works were performed to design SC electrodes by recycling the waste batteries [24–27].

Upcycle of metallic-rich pyrolytic char can be beneficial for improving the structure of electrode materials in supercapacitors by preventing environmental problems caused by e-waste. Based on the above consideration, in this study, it was aimed to obtain carbon-rich metallic char after pyrolysis to use as electrode materials in high–performance supercapacitors (SCs). A novel approach was performed to get non-separating metal fraction from the char and utilize it as metal–carbon source for supercapacitor electrodes. Obtained pyrolytic carbon, C-WPCB was deposited on porous Nickel foam in three different electrolyte 1.5 M H_2SO_4, 3 M KCl, and 1.5 M KOH, respectively, at 1 V for 900 s using two-electrode configuration with respect to the counter Pt electrode.

For the electrochemical measurements, cyclic voltammetry (CV) and galvanostatic charge–discharge (GCD) process was applied. The highest capacitance, energy, and power values were obtained for the electrode deposited in H_2SO_4 electrolyte. The specific capacitance, specific power, and specific energy were found as 39.5 F/g, 25.0 kW/kg, and 16.5 Wh/kg at 5 A/g.

2 Experimental

2.1 Materials

Herein, low-grade waste printed circuit boards (W-PCBs) were converted into pyrolytic carbon and pyrolytic oil through pyrolysis. Solid products were collected as pyrolytic carbon, labeled as C-WPCB, structural characterized, and utilized in supercapacitor electrode.

In this work, low-grade W-PCBs, which were used as feedstock, were provided by Proses Rafinasyon ve Metal Geri Kazanım Makina Sistemleri Company, Turkey and they were shredded together with their components (resistance, relay, capacitor, transistor, heat sink, chip lines, processors) before supplied to the laboratory. The multifarious W-PCBs were fractioned with the help of vibratory sieve shakers (Fritsch, Analysette 3 Spartan) in a measuring range of 1180–63 µm with ASTM standard sieves. The quantitative particle size distribution of W-PCBs was measured, and it was found that the main fractions of W-PCBs have sizes below 180 µm and at 1180 µm as seen in Fig. 1.

2.2 Pyrolysis experiments

Figure 2 shows the flow diagram of pyrolysis process. Pyrolysis experiments were performed under nitrogen atmosphere in a semi-batch type reactor (316 L stainless steel) especially designed for the pyrolysis process. 15 g of W-PCB was placed to the reactor. The reactor was degassed with N_2 gas for 15 min, and then heated up to 500 °C at 20 °C/min ramp and under nitrogen flow rate of 0.01 L/min. During this heating process, volatile gases were transferred to the two-stage cooling chamber where some of them was recovered through condensation. At the end of the pyrolysis experiments, the system was allowed to cool down to the room temperature.

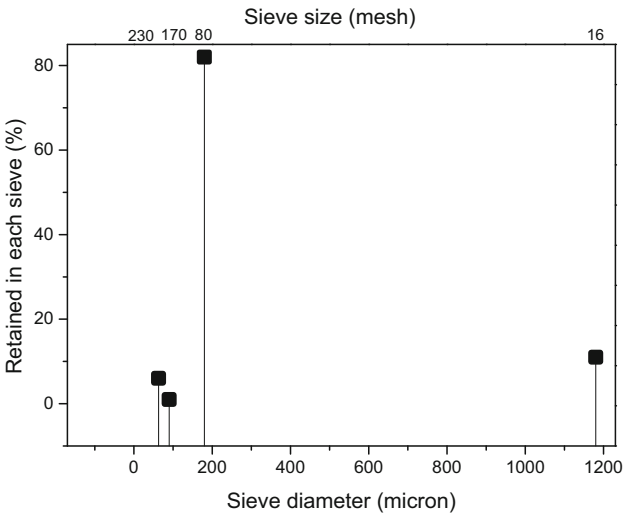

Fig. 1 Sieve analysis of W-PCB

The C-WPCB, which is the pyrolysis residue of W-PCB, was collected from the pyrolysis reactor, and then subjected to structural characterization.

2.3 Characterization

Following the pyrolysis procedure, the collected C-WPCB was structurally characterized by the following well-known techniques:

2.3.1 *Surface morphology*

The morphologies, elemental composition, and elemental mapping were evaluated using a scanning electron microscopy with energy-dispersive spectroscopy (SEM/EDS, ZEISS EVO LS10). Samples were mounted on aluminum stubs using carbon sticky bands and coated with gold.

2.3.2 *Elemental composition*

Energy-dispersive XRF spectroscopy (XRF) is used for elemental analysis of pressed powder W-PCB and C-WPCB samples. XRF analysis was performed on the incinerated char sample. The elements in the Na and U range of the powder sample were identified by helium gas environment with a silicon drift detector.

2.3.3 *Crystalline structures*

The crystalline structure of samples was identified by Powder X-ray diffraction (XRD) analysis performed on Philips Panalytical X'Pert-Pro diffractometer with

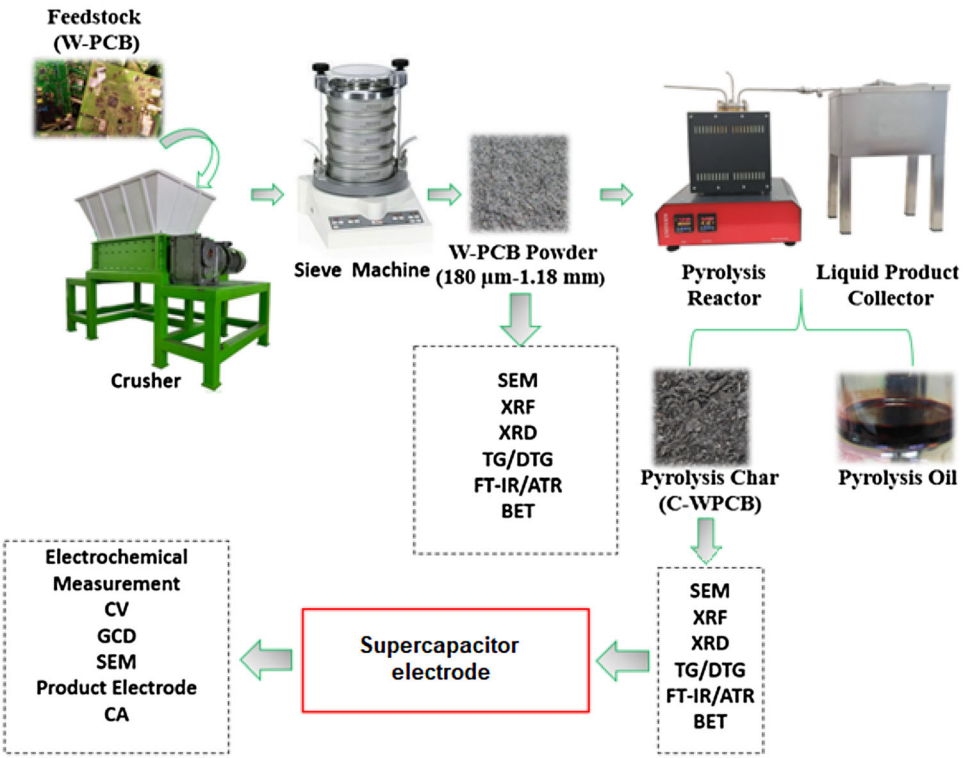

Fig. 2 Flow diagram of pyrolysis process

a Cu K*a* source at the operating parameters of 40 mA and 45 kV, with step size 0.02° and speed 1°/min.

2.3.4 *Chemical bonds*

Fourier Transform Infrared (FTIR) spectroscopy equipped with attenuated total reflection (ATR) analysis was performed to study the identification of chemical bonds available in the samples. The samples were scanned using Spectrum 100, PerkinElmer Fourier transform infrared spectroscopy in the range of 4000–650 cm^{-1} with 4 cm^{-1} resolution.

2.3.5 *Specific surface area*

The N_2 adsorption/desorption isotherm was carried out on Micrometerics Co, USA surface area and porosity analyzer at − 196 °C after evacuation of the samples at 100 °C for 2 h. The specific surface area was determined by using Brunauer–Emmett–Teller (BET) method at a relative pressure of 0.0–0.5 range.

2.3.6 *Combustion characteristics*

The combustion characteristics were studied using SII6000 EXSTAR 6300 (Seiko Instruments, Japan) model TG/DTA simultaneous thermal analyzer under air flow rate of 200 mL/min, at a heating rate of 10 °C/min from ambient temperature to 820 °C. A sample mass of 3.5 ± 0.5 mg was used for experiments.

2.4 Preparation of char dispersion and electrodeposition

Three different aqueous solutions of C-WPCB (acidic-1.5 M H_2SO_4, basic-1.5 M KOH, and neutral-3.0 M KCl) were prepared by putting 7.5 gr powder of C-WPCB into beaker and then 50 mL solute was poured. Each solution was stirred on the magnetic stirrer at 400 rpm for 24 h.

Three porous nickel base electrodes were taken with the dimension of 1 cm × 3 cm. To clean and activate the surface, each electrode was soaked into 37% HCl and stirred for 5 min. After that, they were cleaned with ethyl alcohol. Then, the electrodes were weighed. Chronoamperometric technique was used to deposit the C-WPCB, which was dispersed in different solutions as mentioned above, onto the porous nickel electrode at 1 V for 900 s. After that, the electrodes were weighed, and the active materials deposited on the electrodes in H_2SO_4, KCl, and KOH were measured as 0.2, 0.7, and 1.0 mg, respectively.

The electrodes obtained by this process were waited for 24 h under the room temperature.

2.5 Electrochemical characterization

Electrochemical characterization of each electrode was performed by using Gamry 1010 Potentiostat in 6 M KOH solution as half-cell configuration where each electrode was evaluated with respect to Pt electrode. Cyclic voltammetry (CV) at different scan rates, 20–200 mV/s, and galvanostatic charge–discharge (GCD) at different current densities, 0.5, 1.0, 3.0, and 5.0 A/g, were performed to carry out the electrochemical performance of the electrodes.

3 Results and discussion

3.1 Characterization of waste printed circuit boards

The SEM micrograph of the pyrolytic carbon (C-WPCB) and its elemental composition are shown in Fig. 3a and b where the rod-shape structures spherical and rectangular particles were observed.

Das et al. also observed such rod-shape structures associated with glass fiber materials which indicates the content of Si, O, and Ca elements [28]. According to the EDS analysis, the surface includes Si (17%), O (18%), Ca (6%), Al (5%), Fe (3%), Pb (3%), and Cu (2%). After the pyrolysis, glass fiber materials were remained almost unchanged, and the dimension of rod-shape became smaller. The organic fraction of these plastics was completely decomposed into the carbon [29].

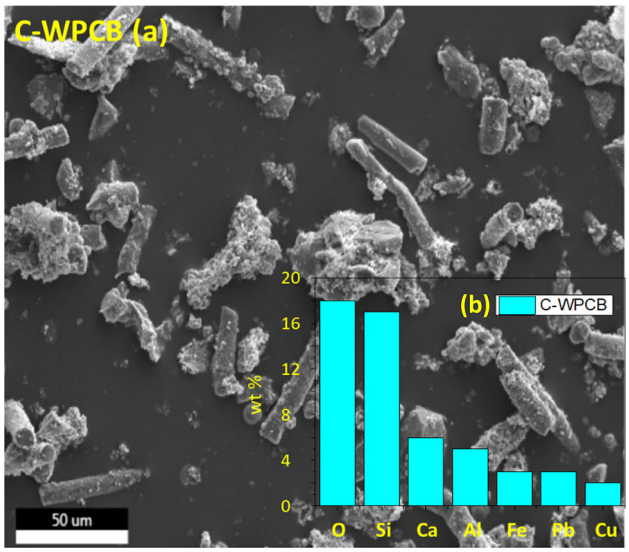

Fig. 3 SEM images of **a** C-WPCB and **b** its elemental composition

Table 1 shows the semi-quantitative XRF analysis results of C-WPCB. The C-WPCB contains many metals such as Si, Ca, Fe, Cu, and Zn, and these results were also confirmed with EDS analyses [30]. Besides, Br (8%) in the sample is due to epoxy resin content [31].

The XRD pattern of the C-WPCB is represented in Fig. 4, in which the peak at 26.84° corresponds to the (002) reflection of carbon with a value of d(002) is 3.321 Å. The reflection around 42.94° corresponds to the (100) plane and indicates sp2-hybridized carbons. The peaks at 49.60° and 42.54° were associated with Fe in the C-WPCB structure. Besides C and Fe, the peak positions at 42.94° and 68.49° correspond to the diffractions from the (111) and (220) planes of Cu with a d spacing of 2.106 and 1.369 Å, respectively [28]. Quan et al. confirmed that the carbon structure obtained from printed circuit board is based on XRD analysis [32].

Figure 5 shows the FTIR spectrums of C-WPCB and W-PCB over the range of 4000–650 cm^{-1}. FTIR spectra revealed that C-WPCB sample was rich in functional groups. Specifically, 3500–3600 cm^{-1} spectral range was attributed to the O–H bond due to the water content in W-PCB sample [18]. The peak at 3067–3000 cm^{-1} was associated with aromatic asymmetric and symmetrical C-H stress vibrations which might be due to the benzene ring skeleton [33]. The bands at 1602–1403 cm^{-1} were attributed to the C–O bonds which may indicate that some of the aromatic structures may be broken down during pyrolysis. Peak detected at 1251 cm^{-1} was considered to be –Si–O–Si which is an indication of glass fiber present in the C-WPCB sample [34]. The vibration

Table 1 Semi-quantitative XRF analysis result of C-WPCB

Components in C-WPCB	wt. (%)
CuO	32
CaO	23
SiO_2	18
FeO	14
Br	8
ZnO	2
Minor elements (Ba, Pb, Ni, Mn, Cr, Ti)	3

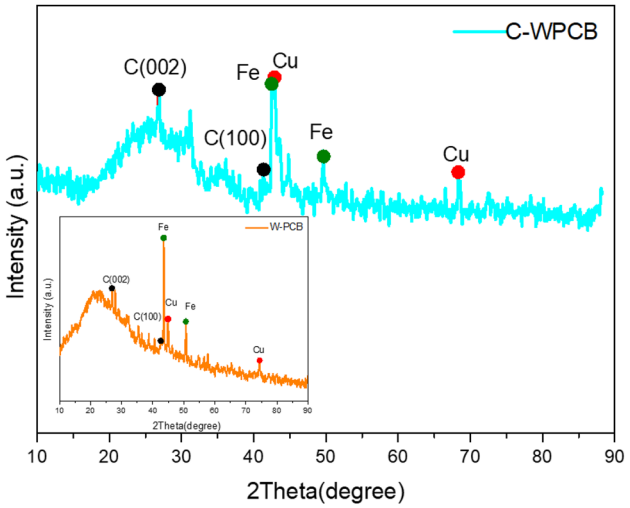

Fig. 4 XRD patterns of C-WPCB and W-PCB

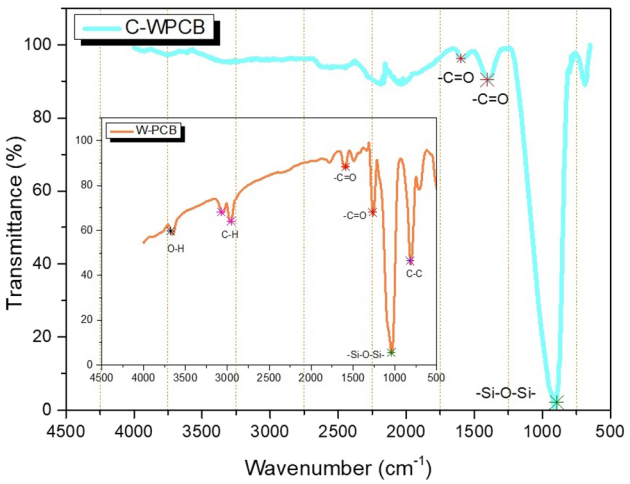

Fig. 5 FTIR spectrum of C-WPCB and W-PCB

peak of C–C at 800.97 cm^{-1} in W-PCB disappeared in C-WPCB after the pyrolysis due to the degradation of epoxy resin [35].

In order to determine the combustion characteristics of C-WPCB, the sample was heated up to 900 °C at 10 °C/min rate under air atmosphere, and the related TG/DTG curves are given in Fig. 6 where the thermal degradation with three consequent steps was observed clearly. The first degradation step is related with the moisture evaporation (30–150 °C) and 2.2% weight loss was occurred. The weight loss, which was predominantly in the temperature range of 250 to 510 °C in the second stage, was associated with CO and CO_2 release. In the last stage (400–800 °C) of the heating, 14.21% weight loss was observed which is due to the rapid release and combustion of the

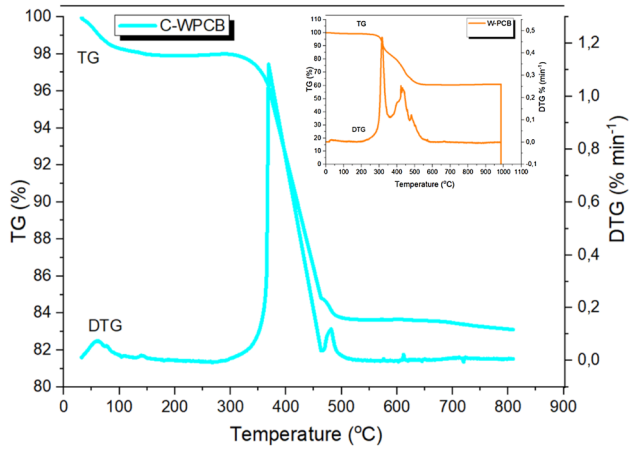

Fig. 6 TG and DTG curves of C-WPCB and W-PCB

C-WPCB volatiles [30]. The residue content was determined as 16.0% from the TG curve. On the other hand, W-PCB combustion took place in four stages as the removal of some low molecular weight volatile gases (25–298 °C), devolatilization (298–450 °C), and char combustion (450–564 °C) as seen in the inset of Fig. 6. Carbon residue combustion appeared with small hump values of 0.074% min^{-1} at 504 °C. A net mass loss of 39.3% was observed due to the rapid release and combustion of the W-PCB volatiles, and residue amount was calculated as 60.7%. The C-WPCB maximum peak was apparently narrow and lay after the W-PCB maximum peak. The maximum mass loss rate of C-WPCB reached 1.32% min^{-1}, which was much higher than that of W-PCB. This situation explains that the C-WPCB has a much higher specific surface area and pore volume than the W-PCB. The porosity in the C-WPCB makes the reactive gas more reachable to the active zone providing better combustibility. Consequently, fixed carbon combustion was the significant combustion process for C-WPCB, while volatilization and gas-phase combustion were other significant processes for W-PCB [36].

BET (Brunauer–Emmett–Teller) surface area and pore volume of W-PCB and C-WPCB were analyzed by N_2 adsorption at 100 °C and 2 h, and the results are summarized in Table 2. The surface area increased to almost 70-fold after pyrolysis of W-PCB which indicates that the pyrolysis process increases the porosity of the surface. In addition, the pore volume also increased and the pore sizes are less than 2 nm [37]. As a conclusion, during the pyrolysis, volatized gas was evolved from W-PCB, and a

Table 2 N_2 sorption properties feedstock and metallic pyrolytic carbon

Sample	Bet surface area (m^2/g)	Pore volume (cm^3/g) × 10^{-4}	Average pore size (nm)
W-PCB	0.26	1.13	1.85
C-WPCB	18.56	37.65	1.28

carbon-rich solid residue was obtained with higher surface area.

3.2 Electrochemical measurements

The CV curves of the Ni electrodes, which were electrochemically coated by C-WPCB together with uncoated one, are represented in Fig. 7. The CV curves of all electrodes were taken in 6 M KOH solution with respect to Pt electrode.

It is clearly seen in Fig. 7 that coating the Ni electrodes with C-WPCB increased the current levels in all situations but it is more pronounced for the electrode coated in acidic medium, H_2SO_4. This result shows that depositing C-WPCB on the Ni electrodes increased the porosity thus the surface area. In addition, the oxidation peaks are most prominent for the electrode coated in KOH which may be due to the involvement of adsorbed hydroxyl groups on the electrode surface [38] and reactants in the coating due to the ingredients of the char [39]. Not only the Ni atoms but also other elements in the char, which deposited on Ni surface during the chronoamperometry process, may have oxidation reaction.

To understand the reason of the CV curve expansions due to deposition of C-WPCB on the Ni electrodes, microstructural topography and elemental analysis of the electrodes were determined by SEM and SEM–EDS, respectively, as given in Figs. 8 and 9.

Grown phases are clearly seen in the SEM images as shown in Fig. 8. On each of the electrodes, elements in char were grown as nanoparticles, so these phases enable higher specific surface area depending on the particle size. Also, some nanopores and nanogaps were seen on the surfaces. Based on the solution by which char was saluted and electrodeposited, the particle forms and dispersions were varied. Nevertheless, the specific surface area of the electrodes was positively affected by each secondary phase formations. The elemental composition of the electrodes was determined by SEM–EDS and the results are shown in Fig. 9. It is clearly seen that C atoms were deposited in all situations, while Fe

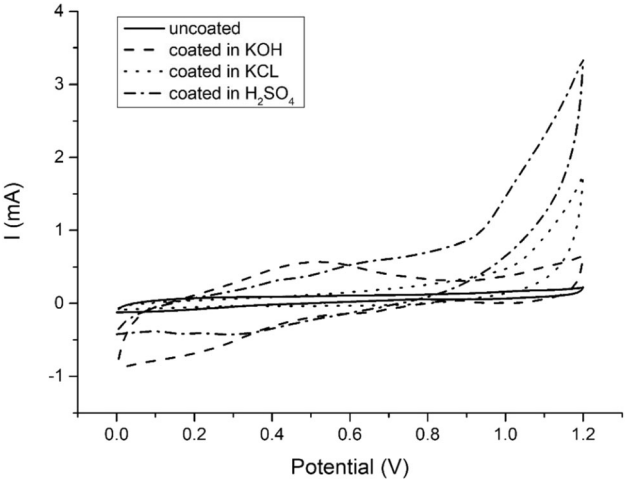

Fig. 7 CV curves of uncoated and coated Ni electrodes at 200 mV/s. The coating of the Ni electrodes was performed by dispersing C-WPCB in aqueous solutions of KOH, KCl, and H_2SO_4

atoms only were deposited on the electrodes modified in KOH and KCl.

It is known that C element is non-faradic but Fe may be participated in electrochemical reactions, as it is faradic. Despite being non-faradic, C may contribute to electrochemical performance by covering the surface and expanding the surface area. [40]. In addition, S atoms are present and the oxygen amount is bigger on the surface of the Ni electrode coated in aqueous solution of H_2SO_4.

The specific capacitance of the electrodes can be determined by either CV curves or GCD. To understand the charge–discharge characteristics and specific capacitance values, GCD measurements were performed for each electrode, and the specific capacitances of the electrodes were calculated by dividing the capacitance values obtained from Gamry software with the mass of the active material coated on the Ni electrode.

The GCD figures of the electrodes deposited in KOH, KCl, and H_2SO_4 at 1A/g are represented in Fig. 10. Here, the deposited electrodes in KCl and KOH electrolytes have considerably longer charge–discharge times than that of in H_2SO_4. In addition, the multi-step charging process seen in the electrode

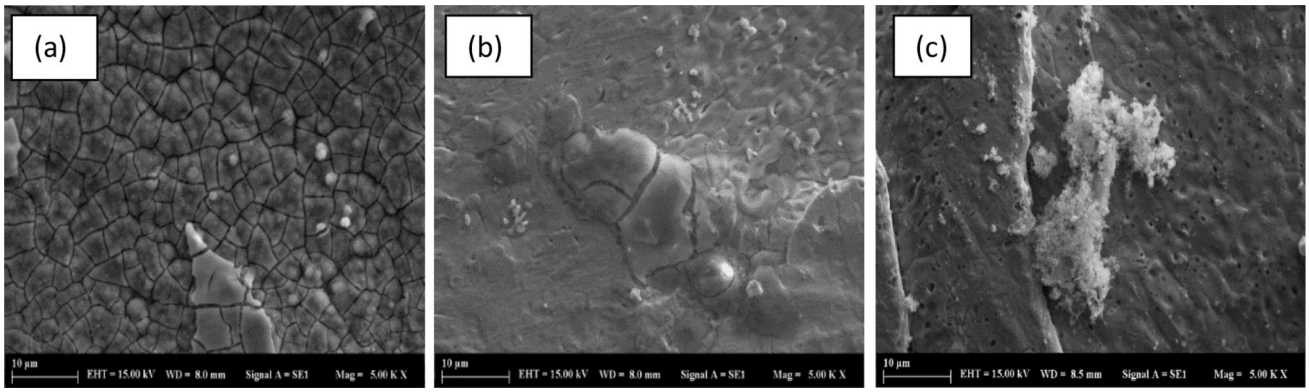

Fig. 8 SEM images of Ni electrodes on which the C-WPCB was deposited in **a** H_2SO_4, **b** KOH, and **c** KCl, respectively

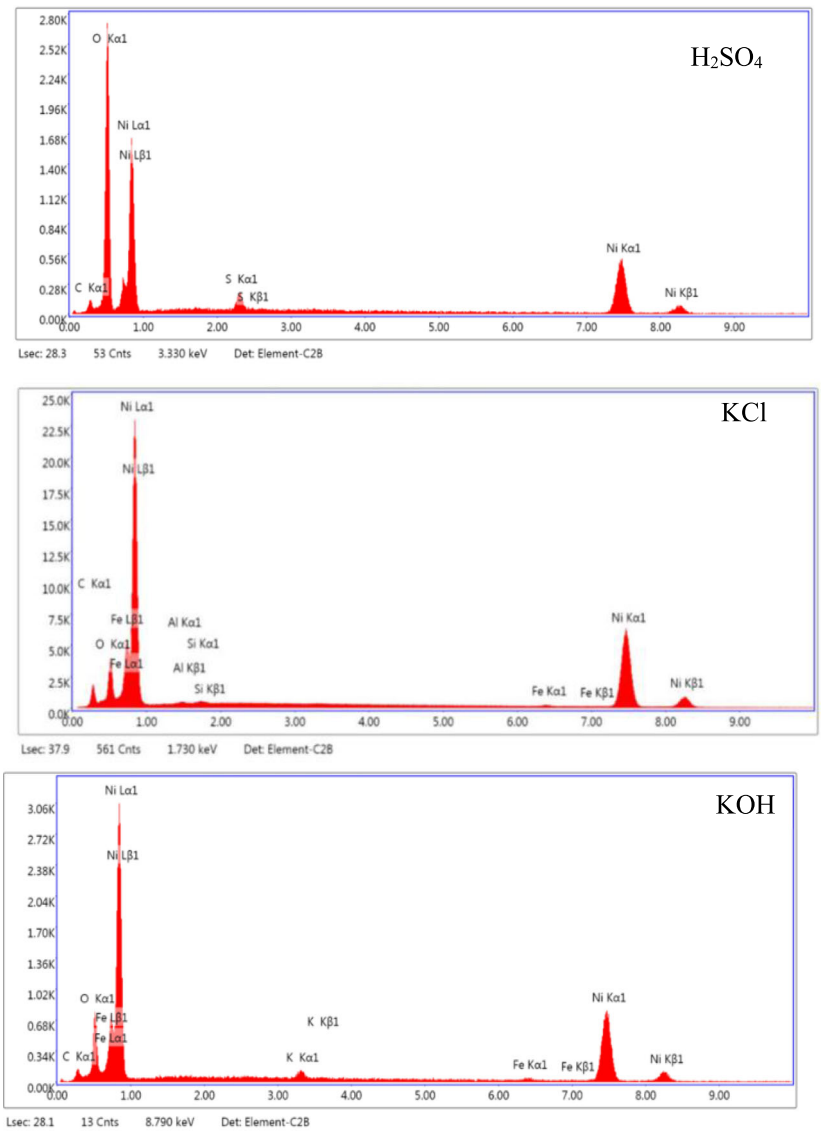

Element	Weight %
C	1.8
O	27.1
S	2.2
Ni	68.9

Element	Weight %
C	4.2
O	4.8
Fe	0.7
Ni	90.3

Element	Weight %
C	1.7
O	7.3
K	1.7
Fe	1.4
Ni	87.9

Fig. 9 EDS analysis of the electrodes coated with C-WPCB dispersed in H_2SO_4, KOH, and KCl, respectively

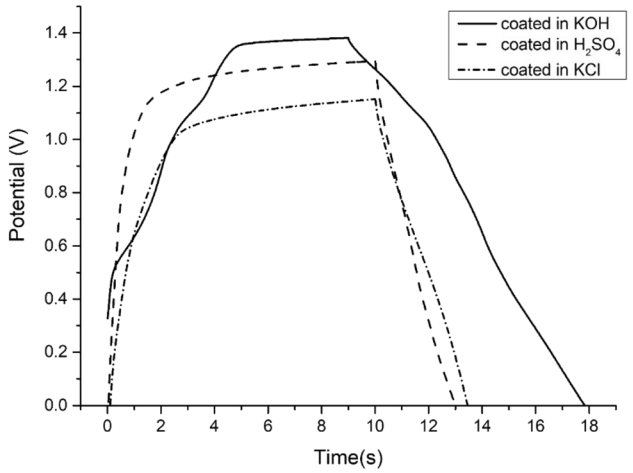

Fig. 10 Charge–discharge curves of electrodes coated with C-WPCB dissolved in KOH, H_2SO_4, and KCl at 1.0 A/g

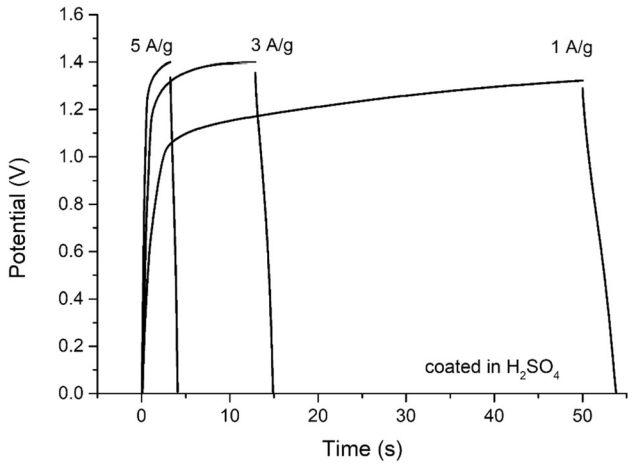

Fig. 11 Charge–discharge curves of electrodes coated with C-WPCB dissolved in H_2SO_4 at 1.0, 3.0, and 5.0 A/g current densities

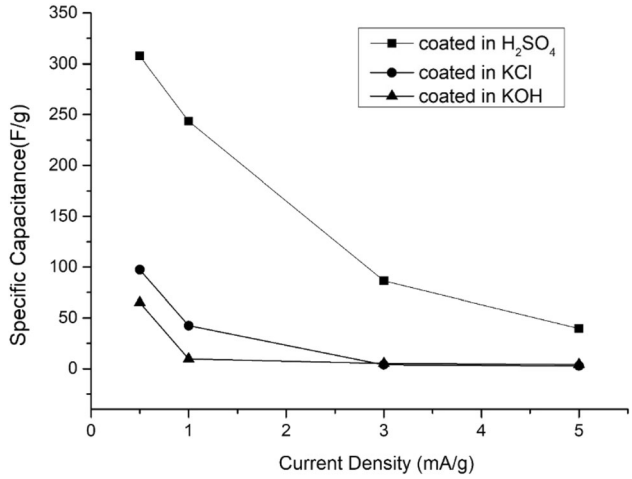

Fig. 12 Specific capacitances of the three electrodes at 0.5, 1.0, 3.0, and 5.0 A/g current densities

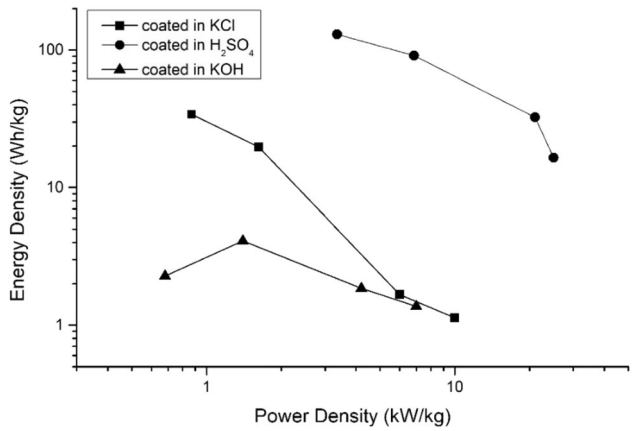

Fig. 13 Specific energy and specific power values of the electrodes deposited in KCl, H_2SO_4, and KOH electrolytes

coated in KOH is probably due to the inefficient deposition of C-WPCB on the Ni surface.

The GCD curves of the electrode coated in H_2SO_4 at 1.0, 3.0, and 5.0 A/g current densities are represented in Fig. 11. As expected, it is seen that charge–discharge process takes less time at high current densities which shows that ion transfer between the electrolyte and electrode takes place in a shorter time.

Calculated specific capacitances of the electrodes are shown in Fig. 12 as a function of current density. It is clearly seen that the specific capacitance values for the three electrodes decrease toward higher current densities. This is an expected result that the capacitance is directly proportional to the charge–discharge time as can be seen in Eq. 1. Since this time will be longer at low current densities due to the slower ion transfer between the electrodes, higher capacitance values were obtained.

The high capacitance observed especially for the electrode coated in H_2SO_4 may be due to the coating the surface more toughly than the others, while the electrode was loosely coated in KOH as seen in the SEM images given in Fig. 8 and EDS analysis. Thus, the specific surface area was increased for the electrode prepared in H_2SO_4 which enables more ion transfer when compared with other electrodes. In addition, it has also been stated that oxygen defects increase the capacitance of supercapacitors [41, 42]. As can be seen in the EDS analysis given in Fig. 9, this change is mostly dominant for the electrode

prepared in H_2SO_4. This finding supports the capacitance to be higher for this electrode.

Specific energy and specific power density values were calculated by using the following equations, respectively.

$$E = \frac{1}{2}C(\Delta V)^2, \quad (1)$$

$$P = \frac{E}{\Delta t}. \quad (2)$$

Depending on the specific energy and the specific power values, the characteristics of the electrodes can be determined where the specific power and the energy values must be in the interval of 0.1–50.0 kW/kg and 0.1–10.0 Wh/kg, respectively [43]. It is clearly seen in Fig. 13 that both the specific energy and the specific power values of the electrodes coated in KCl and H_2SO_4 are higher at all current densities than the electrode coated in KOH. This ratio is especially evident in slower current densities. At 0.5 A/g, specific energy of the electrode deposited in H_2SO_4 is 130 Wh/kg and 3.4 kW/kg while they are 34.1 Wh/kg and 0.87 kW/kg for the electrolyte deposited in KCl. These results clearly show that the electrodes prepared in this study are in the interval for the supercapacitors where the specific power and the specific energy values are in the range of 0.1–50.0 kW/kg and 0.1–10.0 Wh/kg, respectively [43]

4 Conclusion

Metallic pyrolytic carbon was successfully obtained from waste PCBs by using pyrolysis and deposited electrochemically on Ni foam electrode, in acidic, basic, and neutral solutions. Each electrode exhibited almost pseudocapacitive property which lead higher energy density due to the faradic reactions, It was observed that the electrode prepared in acidic solution, H_2SO_4, has better electrochemical performance which is due to more porous structure than the others. Moreover, at the same potential ranges, electrodes deposited in H_2SO_4 can reach higher current densities than those of KOH and KCl.

It was shown that the pyrolysis residue with metal fraction which is non-separated from char can be used as an active material instead of active carbon in supercapacitors due to its porous carbon structure, high surface area, rich functional groups, and conductivity.

Author contributions

AKF and ÖY contributed toward conceptualization; HHC, AKF, ÖY, and KA contributed toward methodology; HHC, İY, KA, ÖY, and AG contributed toward formal analysis and investigation; HHC, AKF, ÖY, and AG contributed toward writing—original draft preparation; AKF, ÖY, and AG contributed toward writing—review and editing; and AKF contributed toward supervision.

Funding

This work was supported by Yıldız Technical University Scientific Research Projects Coordinator's project numbered FBA-2021-4087.

Data availability

Data will be made available on requested.

Declarations

Conflict of interest All the authors do not have any possible conflicts of interest.

References

1. J. Wang, Z. Xu, Disposing and recycling waste printed circuit boards: disconnecting, resource recovery, and pollution control. Environ. Sci. Technol. (2015). https://doi.org/10.1021/es504833y
2. R. Akram et al., Trends of electronic waste pollution and its impact on the global environment and ecosystem. Environ. Sci. Pollut. Res. Int. **26**(17), 16923–16938 (2019). https://doi.org/10.1007/S11356-019-04998-2
3. S.M. Abdelbasir, C.T. El-Sheltawy, D.M. Abdo, Green processes for electronic waste recycling: a review. J. Sustain. Metall. **4**(2), 295–311 (2018). https://doi.org/10.1007/S40831-018-0175-3
4. C.H. Lee, C.T. Chang, K.S. Fan, T.C. Chang, An overview of recycling and treatment of scrap computers. J. Hazard. Mater.

114(1–3), 93–100 (2004). https://doi.org/10.1016/J.JHAZMAT.2004.07.013

5. M. Tatariants, S. Yousef, R. Sidaraviciute, G. Denafas, R. Bendikiene, Characterization of waste printed circuit boards recycled using a dissolution approach and ultrasonic treatment at low temperatures. RSC Adv. **7**(60), 37729–37738 (2017). https://doi.org/10.1039/C7RA07034A
6. W. Utetiwabo et al., Electrode materials derived from plastic wastes and other industrial wastes for supercapacitors. Chinese Chem. Lett. **31**(6), 1474–1489 (2020). https://doi.org/10.1016/j.cclet.2020.01.003
7. W. Liu, J. Xu, J. Han, F. Jiao, W. Qin, Z. Li, Kinetic and mechanism studies on pyrolysis of printed circuit boards in the absence and presence of copper. ACS Sustain. Chem. Eng. (2019). https://doi.org/10.1021/acssuschemeng.8b03382
8. G. Jie, L. Ying-Shun, L. Mai-Xi, Product characterization of waste printed circuit board by pyrolysis. J. Anal. Appl. Pyrolysis (2008). https://doi.org/10.1016/j.jaap.2008.08.007
9. J. Hao, H. Wang, S. Chen, B. Cai, L. Ge, W. Xia, Pyrolysis characteristics of the mixture of printed circuit board scraps and coal powder. Waste Manag. (2014). https://doi.org/10.1016/j.wasman.2013.10.043
10 I. Hussain et al., Binder-free trimetallic phosphate nanosheets as an electrode: theoretical and experimental investigation. J. Power Sources **513**, 230556 (2021). https://doi.org/10.1016/j.jpowsour.2021.230556
11. R. Zhou, X. Li, H. Pang, VOx/VSx@Graphene nanocomposites for electrochemical energy storage. Chem. Eng. J. **404**, 126310 (2021). https://doi.org/10.1016/J.CEJ.2020.126310
12 S. Huang, X. Zhu, S. Sarkar, Y. Zhao, Challenges and opportunities for supercapacitors. APL Mater. (2019). https://doi.org/10.1063/1.5116146
13. S. Zhao et al., Flexible Nb4C3Tx Film with large interlayer spacing for high-performance supercapacitors. Adv. Funct. Mater. **30**(47), 1–8 (2020). https://doi.org/10.1002/adfm.202000815
14 R.T. Ginting, M.M. Ovhal, J.W. Kang, A novel design of hybrid transparent electrodes for high performance and ultra-flexible bifunctional electrochromic-supercapacitors. Nano Energy **53**, 650–657 (2018). https://doi.org/10.1016/j.nanoen.2018.09.016
15 I. Hussain et al., High entropy alloys as electrode material for supercapacitors: a review. J. Energy Storage **44**, 103405 (2021). https://doi.org/10.1016/J.EST.2021.103405
16 C. Chen Nie et al., Cleaner utilization of non-metallic components in separation tailings of waste printed circuit board: pyrolysis oil, calorific value and building aggregate. J. Clean. Prod. **258**, 120976 (2020). https://doi.org/10.1016/j.jclepro.2020.120976
17 W. Chen, Y. Chen, Y. Shu, Y. He, J. Wei, Characterization of solid, liquid and gaseous products from waste printed circuit board pyrolysis. J. Clean. Prod. **313**, 127881 (2021). https://doi.org/10.1016/j.jclepro.2021.127881
18. Y. Shen, X. Chen, X. Ge, M. Chen, Thermochemical treatment of non-metallic residues from waste printed circuit board: pyrolysis vs. combustion. J. Clean. Prod. **176**, 1045–1053 (2018). https://doi.org/10.1016/j.jclepro.2017.11.232
19. Y.H. Ke, E.T. Yang, X. Liu, C.L. Liu, W.S. Dong, Preparation of porous carbons from non-metallic fractions of waste printed circuit boards by chemical and physical activation. Xinxing Tan Cailiao/New Carbon Mater. **28**(2), 108–113 (2013). https://doi.org/10.1016/S1872-5805(13)60069-4
20. R.R. Rajagopal, L.S. Aravinda, R. Rajarao, B.R. Bhat, V. Sahajwalla, Activated carbon derived from non-metallic printed circuit board waste for supercapacitor application. Electrochim. Acta **211**, 488–498 (2016). https://doi.org/10.1016/j.electacta.2016.06.077
21. H. Qin et al., Non-metallic printed circuit board waste derived carbon for the supercapacitor electrode material. Micro Nano Lett. **15**(3), 168–171 (2020). https://doi.org/10.1049/mnl.2018.5743
22 A. Dutta, J. Mahanta, T. Banerjee, Supercapacitors in the light of solid waste and energy management: a review. Adv. Sustain. Syst. (2020). https://doi.org/10.1002/adsu.202000182
23 G. Nagaraju, S.C. Sekhar, J.S. Yu, Utilizing waste cable wires for high-performance fiber-based hybrid supercapacitors: an effective approach to electronic-waste management. Adv. Energy Mater. (2018). https://doi.org/10.1002/aenm.201702201
24. E. Aboelazm, G. A. M. Ali, K. Feng Chong, E. A. Aboelazm, Cobalt oxide supercapacitor electrode recovered from spent lithium-ıon battery nonlinear modeling view project waste recycling technologies for nanomaterials manufacturing view project. Chem. Adv. Mater. 3(4), 67–74 (2018) Cobalt oxide supercapacitor electrode recovered from spent lithium-ıon battery. http://issrpublishing.com/cam/
25. H. Chen, X. Zhu, Y. Chang, J. Cai, R. Zhao, 3D flower-like CoS hierarchitectures recycled from spent LiCoO2 batteries and its application in electrochemical capacitor. Mater. Lett. **218**, 40–43 (2018). https://doi.org/10.1016/j.matlet.2018.01.144
26. Z. Li, D. Xiao, C. Xu, Z. Li, S. Bi, H. Xu, H. Dou, X. Zhang, MnO2/carbon nanotube free-standing electrode recycled from spent manganese-oxygen battery as high-performance supercapacitor material. J. Mater. Sci. **57**(19), 8818–8827 (2022). https://doi.org/10.1007/s10853-022-07223-7
27 R. Farzana, K. Hassan, V. Sahajwalla, Manganese oxide synthesized from spent Zn–C battery for supercapacitor

electrode application. Sci. Rep. (2019). https://doi.org/10.1038/s41598-019-44778-z
28. S.K. Das, G. Ellamparuthy, T. Kundu, M.K. Ghosh, S.I. Angadi, Critical analysis of metallic and non-metallic fractions in the flotation of waste printed circuit boards. Powder Technol. **389**, 450–459 (2021). https://doi.org/10.1016/j.powtec.2021.05.061
29. P. Evangelopoulos, E. Kantarelis, W. Yang, Experimental investigation of pyrolysis of printed circuit boards for energy and materials recovery under nitrogen and steam atmosphere. Energy Proc. **105**, 986–991 (2017)
30 J. Li, H. Duan, K. Yu, L. Liu, S. Wang, Characteristic of low-temperature pyrolysis of printed circuit boards subjected to various atmosphere. Resour. Conserv. Recycl. (2010). https://doi.org/10.1016/j.resconrec.2009.12.011
31 G. Grause, M. Furusawa, A. Okuwaki, T. Yoshioka, Pyrolysis of tetrabromobisphenol—A containing paper laminated printed circuit boards. Chemosphere (2008). https://doi.org/10.1016/j.chemosphere.2007.11.033
32 C. Quan, A. Li, N. Gao, Thermogravimetric analysis and kinetic study on large particles of printed circuit board wastes. Waste Manag. (2009). https://doi.org/10.1016/j.wasman.2009.03.020
33 W.J. Hall, P.T. Williams, Separation and recovery of materials from scrap printed circuit boards. Resour. Conserv. Recycl. (2007). https://doi.org/10.1016/j.resconrec.2006.11.010
34. Y. Shen, Effect of chemical pretreatment on pyrolysis of non-metallic fraction recycled from waste printed. Waste Manage. **76**, 537–543 (2018)
35. S.-R. Shin, V.D. Mai, D.-S. Lee, Chemical recycling of used printed circuit board scraps: recovery and utilization of organic products. Processes **7**, 22 (2019)
36. Q. Yi et al., Thermogravimetric analysis of co-combustion of biomass and biochar. J. Therm. Anal. Calorim. **112**(3), 1475–1479 (2013). https://doi.org/10.1007/s10973-012-2744-1
37. C. Quan, A. Li, N. Gao, Synthesis of carbon nanotubes and porous carbons from printed circuit board waste pyrolysis oil. J. Hazard. Mater. **179**, 911–917 (2010)
38. G.R. Fu, Z.A. Hu, L. Xie, X.Q. Jin, Y.L. Xie, Y.X. Wang et al., Electrodeposition of nickel hydroxide films on nickel foil and its electrochemical performances for supercapacitor. Int. J. Electrochem. Sci. **4**(8), 1052 (2009)
39. H. Chen, S. Zhou, L. Wu, Porous nickel hydroxide–manganese dioxide-reduced graphene oxide ternary hybrid spheres as excellent supercapacitor electrode materials. ACS Appl. Mater. Interfaces. **6**(11), 8621–8630 (2014)
40. L. Mao, C. Guan, X. Huang, Q. Ke, Y. Zhang, J. Wang, 3D graphene-nickel hydroxide hydrogel electrode for high-performance supercapacitor. Electrochim. Acta **196**, 653–660 (2016). https://doi.org/10.1016/j.electacta.2016.02.084
41. D.C. Cronemeyer, M.A. Gilleo, The optical absorption and photoconductivity of rutile. Phys. Rev. **82**(6), 975–976 (1951). https://doi.org/10.1103/PHYSREV.82.975
42 A.S. Etman, L. Wang, K. Edström, L. Nyholm, J. Sun, Molybdenum oxide nanosheets with tunable plasmonic resonance: aqueous exfoliation synthesis and charge storage applications. Adv. Funct. Mater. **29**(4), 1806699 (2019). https://doi.org/10.1002/adfm.201806699
43. H. Jung, N. Venugopal, B. Scrosati, Y. Sun, A high energy and power density hybrid supercapacitor based on an advanced carbon-coated Li4Ti5O12 electrode. J. Power Sources **221**, 266–271 (2013). https://doi.org/10.1016/j.jpowsour.2012.08.039